

# Single magnetic impurities in the Kane-Mele model

Florian Goth, David J. Luitz, and Fakher F. Assaad

*Institut für Theoretische Physik und Astrophysik,  
Universität Würzburg, Am Hubland, D-97074 Würzburg, Germany*

(Dated: October 29, 2018)

The realization of the spin-Hall effect in quantum wells has led to a plethora of studies regarding the properties of the edge states of a two-dimensional topological insulator. These edge states constitute a class of one-dimensional liquids, called the helical liquid, where an electron's spin quantization axis is tied to its momentum. In contrast to one dimensional conductors, magnetic impurities — below the Kondo temperature — cannot block transport and one expects the current to circumvent the impurity. To study this phenomenon, we consider the single impurity Anderson model embedded into an edge of a Kane-Mele ribbon with up to  $512 \times 80$  sites and use the numerically exact continuous time quantum Monte Carlo method (CTQMC) to study the Kondo effect. We present results on the temperature dependence of the spectral properties of the impurity and the bulk system that show the behaviour of the system in the various regimes of the Anderson model. A view complementary to the single particle spectral functions can be obtained using the spatial behaviour of the spin spin correlation functions. Here we show the characteristic, algebraic decay in the edge channel near the impurity.

PACS numbers: 71.10.Fd, 05.10.Ln, 05.70.Ln

## I. INTRODUCTION

Numerical studies of variants of the Kane-Mele model<sup>1</sup> have recently been pursued with increasing interest<sup>2–6</sup> since it can be used as a theoretical framework to study correlation effects in quantum spin-Hall insulators, or two-dimensional (2D) topological insulators (TIs)<sup>7</sup>. A characteristic feature is the formation of metallic edge states at the boundary of the system, which are robust to external perturbations provided that time reversal symmetry is not broken.<sup>8</sup> They form a helical liquid, such that the electrons' spin is tied to its direction of motion<sup>9</sup>.

A particularly interesting perturbation of the helical edge state is the introduction of magnetic impurities interacting with the edge — a problem usually modeled by an  $S = \frac{1}{2}$  local spin that is coupled to the helical liquid. Due to the one-dimensional (1D) nature of the edge this problem has been studied extensively with bosonization techniques with variable Luttinger liquid parameter accounting for correlation effects in the helical edge state<sup>10–13</sup>. The Kondo effect in three dimensional TIs has been studied in Refs.<sup>14–17</sup>. Returning to the 2D case and in the weak coupling regime with respect to electronic correlations on the edge, the formation of the Kondo singlet will effectively remove sites, thereby redefining the topology of the slab and the flow of the edge state. The aim of this paper is to study the temperature dependence of this effect by computing, among other quantities, the site dependent density of states. To do so, we will set out to model the magnetic impurity using the single impurity Anderson model<sup>18</sup> which accounts for a single localized energy level that hybridizes with the states of the TI and has an on-site Coulomb repulsion, while sites in the bulk are assumed to be noninteracting. For non-vanishing Hubbard-interaction this model enables us to trace the progression from the high-temperature regime

over the development of the local moment towards the formation of the Kondo singlet. We achieve this with the numerically exact interaction expansion continuous time Quantum Monte Carlo (CT-INT) algorithm introduced by Rubtsov et al.<sup>19–21</sup> which is particularly suitable for the study of impurity problems, since noninteracting bath sites (the TI) do not count towards the computational complexity of the algorithm and can be integrated out. To access the single particle properties of the bath we calculate the self-energy on the impurity and then calculate the bath Green's functions using Dyson's equation. This allows us to exhibit the deflection of the edge state at the impurity by looking at the spectral signatures arising in the bulk spectral functions due to the emerging Kondo effect on the impurity. Towards the end we progress from the one-particle spectral functions to a two-particle quantity, the spatially resolved, equal-time, spin spin correlation function. Using this quantity, we can inquire the spatial extent of the Kondo screening cloud in the bulk and along the edge.

## II. THE MODEL

The Kane-Mele model was first proposed as a candidate for a possible quantum spin-Hall effect in graphene and its Hamiltonian is given by

$$H_{\text{KM}} = H_t + H_\lambda, \quad (1)$$

with

$$\begin{aligned} H_t &= -t \sum_{\vec{i}\sigma} a_{i\sigma}^\dagger (b_{i\sigma} + b_{i+a_1-\vec{a}_2,\sigma} + b_{i-\vec{a}_2,\sigma}) + h.c. \\ H_\lambda &= \lambda \sum_{\vec{i}\sigma} \sigma \left[ i a_{i\sigma}^\dagger (a_{i+a_1,\sigma} + a_{i-\vec{a}_2,\sigma} + a_{i+a_2-\vec{a}_1,\sigma}) \right. \\ &\quad \left. - i b_{i\sigma}^\dagger (b_{i+a_1,\sigma} + b_{i-\vec{a}_2,\sigma} + b_{i+a_2-\vec{a}_1,\sigma}) \right] + h.c. \end{aligned}$$

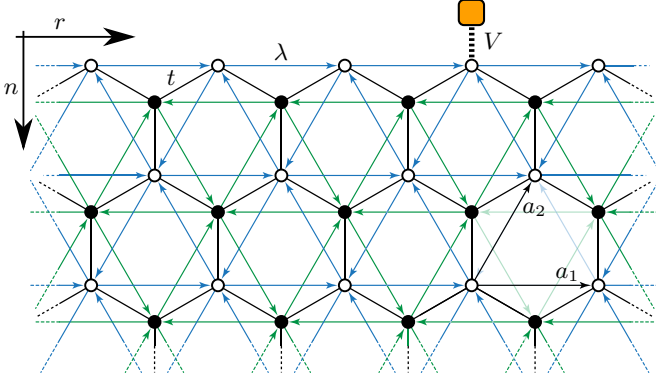


FIG. 1. (Color online) The ribbon is periodic along the  $r$ -direction and at site  $r = 0$ ,  $n = 0$  the orange box denotes the impurity orbital which couples with a matrix element  $V$ . Sublattice  $A$  is denoted by open circles and sublattice  $B$  by filled circles.  $a_1$  and  $a_2$  denote the unit vectors of the honeycomb lattice.

$a_{i\sigma}$  and  $b_{i\sigma}$  denote fermionic operators acting on the respective sublattice and, to account for edge states, we consider this model on a slab geometry. The boundary conditions are periodic in  $r$ -direction – the corresponding number of sites is denoted by  $N_x$  – and open in  $n$ -direction with a length of  $N_y$  sites.  $\lambda$  is the strength of the spin-orbit interaction and the hopping  $t$  is set to  $t = 1$  for everything that follows. The effect of electron-electron interactions in graphene was studied in Ref.<sup>22–24</sup>. Although it turned out that in graphene the spin-orbit coupling is too small to observe the QSH state, the model can still be used as an effective Hamiltonian for this topological state of matter. This model is related to the spinless Haldane model that shows a quantum Hall effect but breaks time reversal invariance (TRI)<sup>25</sup>. The Kane-Mele model can be understood as two copies of the Haldane model while preserving time-reversal symmetry and exhibiting a quantum spin-Hall effect. Into this bath system we embed an impurity at an edge. The impurity's Hamiltonian  $H_{\text{imp}}$  is given by

$$H_{\text{imp}} = H_0 + H_U \quad (2)$$

with

$$H_0 = \epsilon_d \sum_{\sigma} d_{\sigma}^{\dagger} d_{\sigma} + V \sum_{\sigma} (a_{0,\sigma}^{\dagger} d_{\sigma} + d_{\sigma}^{\dagger} a_{0,\sigma})$$

$$H_U = U \left( n_{\uparrow}^d - \frac{1}{2} \right) \left( n_{\downarrow}^d - \frac{1}{2} \right).$$

Here,  $\epsilon_d$  denotes the energy of the dot,  $U$  the Hubbard interaction and  $V$  the hybridization between the first bath site and the impurity.  $d_{\sigma}$  denotes fermionic operators acting on the impurity. We have chosen a symmetric representation of the Hubbard interaction that sets the chemical potential to zero for the half-filled case. We note that the impurity Hamiltonian obeys time reversal symmetry together with the bath.

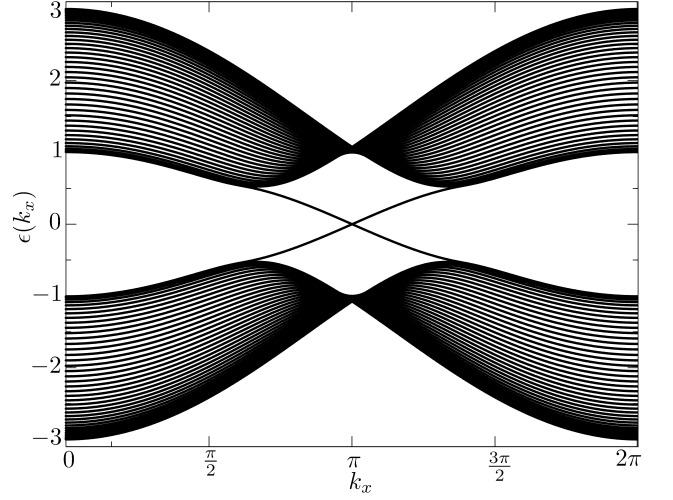


FIG. 2. Spectrum of the Kane-Mele model. Here we have used  $N_x = 512$ ,  $N_y = 80$  and  $\lambda = 0.1$ , which constitute our “canonical values” in the following. Visible are the different bands due to the “orbitals” in  $n$ -direction, as well as the famous edge states crossing at the Fermi energy.

### III. SUMMARY OF BATH PROPERTIES

As already mentioned, the bath model  $H_{\text{KM}}$  exhibits the so-called edge states which, as the name implies, are localized at the edges. Since we attach the impurity to a site belonging to an edge we revisit some properties of the bath. We refer to anything outside of the impurity as bath and everything in the bath that is not dominated by the edge state as bulk. The edge states correspond to the states in the energy spectrum of Fig. 2 that cross at the Fermi energy,  $\epsilon(k_x) = 0$ , and enable gapless electronic excitations at the edge. These edge states constitute a helical liquid where the spin of an electron is coupled to the direction of propagation, hence an interaction flipping the spin reverses its momentum. Since we will argue quite a bit with the help of the spectral functions we point out the general structure of  $A_n(r, \omega)$  here. It is

$$A_n(r, \omega) = A_n^0(\omega) + B_n(r, \omega, V) + C_n(r, \omega, \Sigma(\omega)) \quad (3)$$

with the impurity independent background  $A_n^0(\omega)$ , a term  $B_n(r, \omega, V)$  that depends on the hybridization  $V$  between lattice and impurity and the contribution  $C_n(r, \omega, \Sigma(\omega))$  due to the self-energy  $\Sigma(\omega)$  of the impurity. In Fig. 3 we show a site-resolved view onto the spectral functions  $A_n^0(\omega)$  of the bath. The bulge that is visible in the outermost ( $n = 0$ ) spectral functions is the edge state, which has its spectral weight centered around  $\omega = 0$ . Since we consider the system without an impurity we have translation invariance along the  $r$ -direction. For comparison we show in Fig. 4 a cut along  $r = 0$  of the same spectral functions. Further into the bulk the gap of the insulator appears. Also we see the odd-even pattern close to the edge. The  $n = 1$  spectral function shows a gap, whereas the  $n = 2$  function shows some remains of

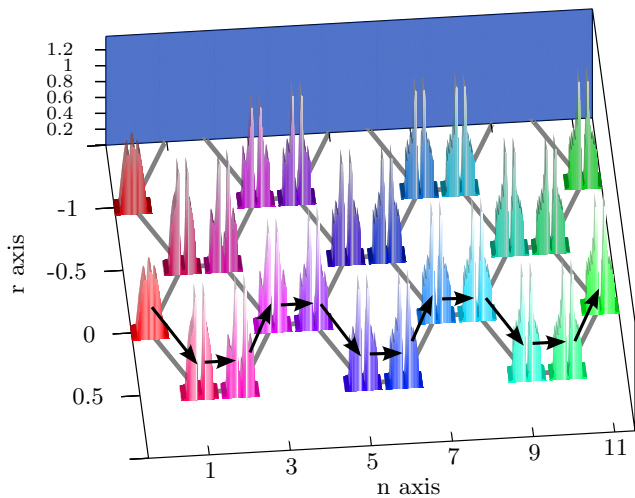


FIG. 3. (Color online) This plot shows a part of the real-space lattice at  $\lambda = 0.1$  where to every lattice point we have attached the spectral function  $A_n^0(\omega)$ . For a given value of  $r$ , the black arrows denote the path that is taken through the lattice if  $n$  is increased. Since the impurity is not yet added we have translation invariance along the  $r$  direction. The bulge of the edge state in the  $n = 0$  spectral functions is clearly visible.

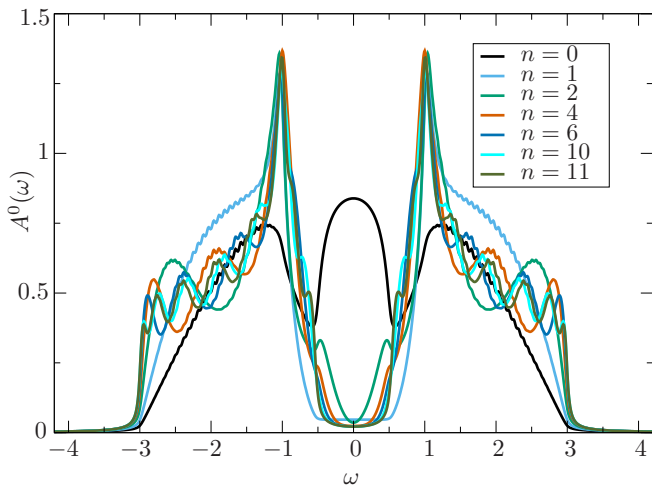


FIG. 4. (Color online) Spectral functions of Fig. 3 for comparison in a more traditional 2D plot. Both plots are from a system with  $N_x = 512$  and  $N_y = 80$  sites at  $\lambda = 0.1$ . The fine wiggles in the spectral functions, as e.g. in  $n = 0$  or  $n = 1$ , are artifacts of the finite system size. The edge state at  $n = 0$  is clearly visible which almost immediately decays farther in the bulk. Having used a finite  $\eta = 4\Delta\omega \approx 0.03$  we have some broadening which prevents the gap of the spectral function from vanishing in the bulk.  $\Delta\omega$  is the resolution of the energy  $\omega$ .

the exponentially decaying edge state.

#### IV. AN UNCORRELATED IMPURITY

Adding to the bath system the uncorrelated impurity given by  $H_0$  at site  $r = 0$  and  $n = 0$  the spectral properties of the system change around the impurity since now the  $B$  - term in Eq. (3) contributes to the spectral functions due to the hybridization  $V$ . From Fig. 5a and Fig. 5b it is visible that right at the impurity the spectral weight of the edge state is drastically reduced. In contrast to the changes due to correlations in Fig. 12a we see that locally this potential poses quite a strong perturbation to  $A(\omega)$ . Since time reversal symmetry is present, single particle backward scattering is prohibited as this would amount to flipping the orientation of the spin. As a consequence, the edge state has to circumvent the potential impurity by deflecting into the bulk. Thus the missing spectral weight reappears at sites further into the bulk. Fig. 5c and Fig. 5d show the change in the spectral function,  $B_n(r, \omega, V)$ , due to the hybridization. The edge state is deformed around the impurity since it acts as a pure potential scatterer for the edge state. This is consistent with the spectral function of the impurity which is just a lorentzian around  $\omega = 0$  similar to the “correlated” spectral function at  $\beta = 0.1$  in Fig. 7a. Although the edge state is protected by symmetry against potential scattering, the effect of the impurity is that it acts as a trap for electrons from the bulk which can then in turn interact with the electrons of the edge state<sup>10</sup>. An interpretation of the resulting new path of the edge channel is that the site to which the impurity is connected is effectively removed from the lattice. In that sense the deformation of the edge state can be understood as a rerouting along the changed edge of the system. A similar deflection of the edge state around centers of potential scattering has also been reported in 3D TT's.<sup>26</sup>

#### V. A CORRELATED IMPURITY

Now we add the Hubbard interaction  $H_U$  to the impurity which leads us to consider the single impurity Anderson model (SIAM)

$$H = H_{\text{imp}} + H_{\text{KM}} \quad (4)$$

with the bath given by the Kane-Mele model  $H_{\text{KM}}$ . Integrating out the bath electrons we obtain the action

$$S = - \sum_{\sigma} \int_0^{\beta} d\tau \int_0^{\beta} d\tau' d_{\sigma}^{\dagger}(\tau) G_{d,d}^{-1}(\tau - \tau') d_{\sigma}(\tau') \\ + U \int_0^{\beta} d\tau \left( n_{\uparrow}^d(\tau) - \frac{1}{2} \right) \left( n_{\downarrow}^d(\tau) - \frac{1}{2} \right) \quad (5)$$

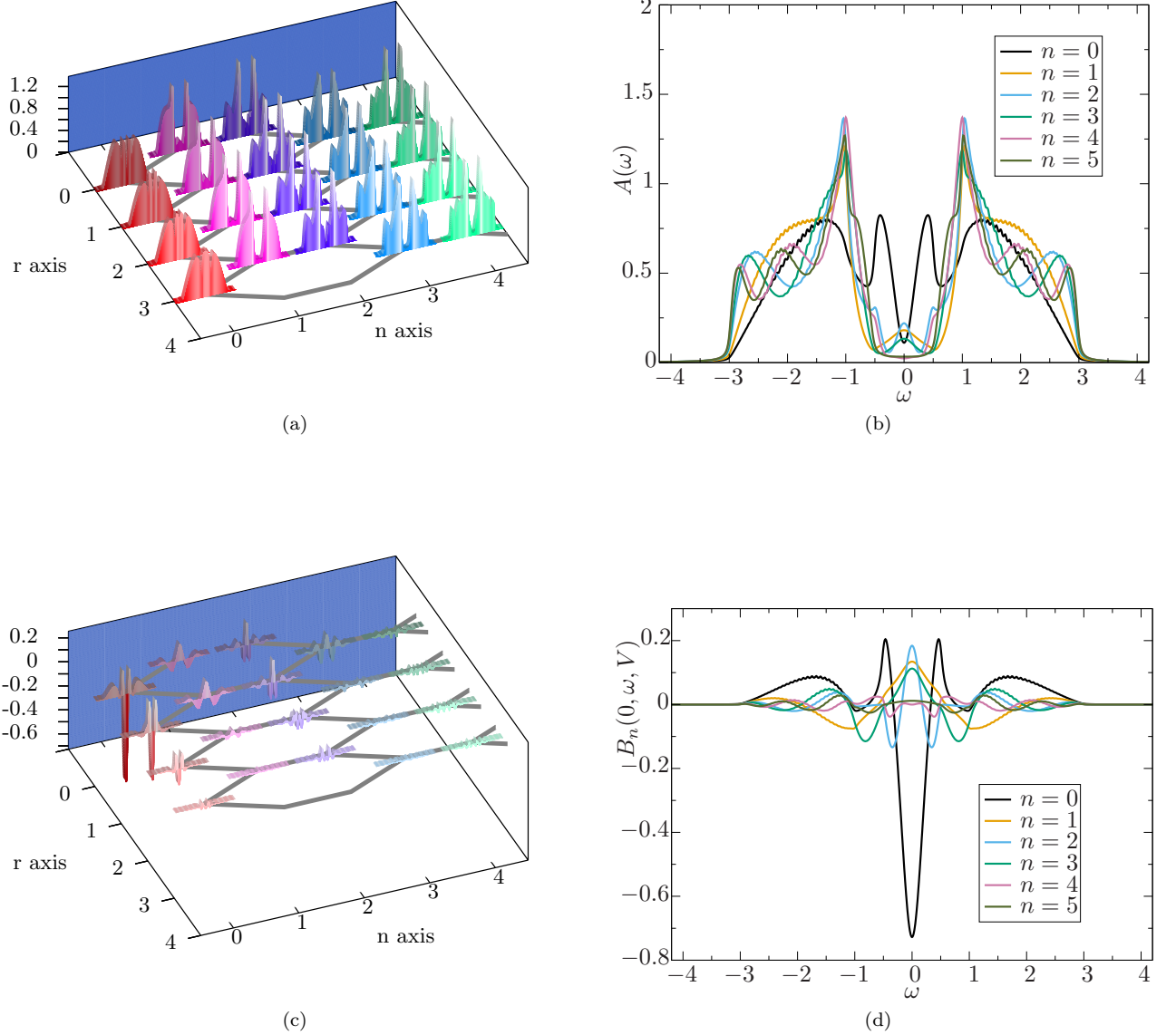


FIG. 5. (Color online) (a) shows the complete spectral functions now with a non-interacting impurity located at  $r = 0$  and  $n = 0$ . The original edge state is deformed into the bulk around the impurity. The missing weight in the  $n = 0$  spectral functions shows up in the  $n = 1, 2$  spectral functions. (b) is a cut of  $A_n(r, \omega)$  along  $r = 0$  that shows the rearrangement of spectral weight from the edge into the bulk. (c) shows  $B_n(r, \omega, V)$ , the effect on the spectral functions attributable to the hybridization  $V$  of the impurity with the edge state. We see large negative contributions to the edge state at the impurity and positive contributions farther into the bulk.  $B_n(r = 0, \omega, V)$  is shown in (d). Obvious is the strong reduction at the site below the impurity ( $r = 0, n = 0$ ) which is shifted to the sites around the impurity.

which is perfectly suitable for an implementation of a numerically exact CTQMC method that expands in the interaction strength  $U$ . The computational effort is reduced if one uses the property that our model is time reversal invariant which leads to a spin-diagonal impurity Green's function  $G_{d,d}$  as detailed in Sec. B for a

general time reversal symmetric Hamiltonian. To at best study the temperature dependence of the above impurity problem, we will compute several quantities. The double occupancy,  $\langle n_{\uparrow}^d n_{\downarrow}^d \rangle$  in Fig. 6a will allow us to track the formation of the local moment and its screening. The same information is essentially contained in the local spin



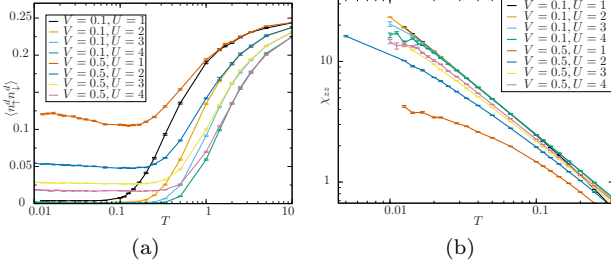


FIG. 6. (Color online) Overview of, (a), the double occupancy and (b),  $\chi_{zz}$ , as a function of temperature  $T = \frac{1}{\beta}$ . The plots of the double occupancy highlight the different regimes. All functions start out at the uncorrelated value  $\langle n_{\uparrow}n_{\downarrow} \rangle = 0.25$  and then fall towards some dip at intermediate temperatures. This dip roughly coincides with the local moment regime. After that, the double occupancy increases slightly up to a saturation which is a signature of the Kondo regime.

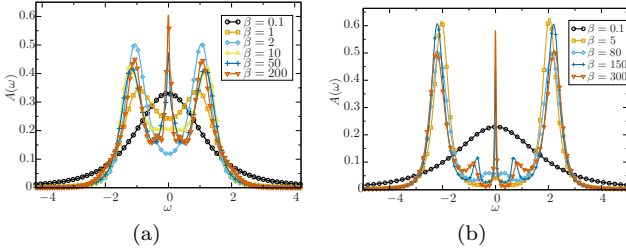


FIG. 7. (Color online) The spectral functions of the dot for (a)  $U = 2$  and (b)  $U = 4$ , both at  $V = 0.5$ . At  $\beta = 0.1$  we see the high-temperature regime with weight centered around zero. Lowering the temperature we cross over into the local moment regime with two clearly separated Hubbard bands at  $\omega \approx \pm \frac{U}{2}$ . Lowering the temperature further we see the emergence of the Kondo resonance at  $\omega = 0$ .

susceptibility

$$\chi_{zz} = \int_0^{\beta} d\tau \langle S^z(\tau) S^z \rangle$$

measured on the impurity and plotted in Fig. 6b. Due to TRI it is sufficient to consider only  $\chi_{zz}$  since the other components are degenerate.

To study the deflection of the edge state as well as the formation of the Kondo resonance, we also compute the site dependent single particle density spectral function

$$A_n(r, \omega) = -\frac{1}{\pi} \text{Im}(G_n(r, \omega + i\eta)) \quad (6)$$

for a small  $\eta$  from the bath Green's function  $G_n(r, z)$  at site  $(r, n)$ . To obtain the spectral functions of the bath lattice we analytically continue the impurity self-energy to real frequencies and use Dyson's equation to access the lattice spectral functions as detailed in appendix A. Additionally we get access to the term  $C_n(r, \omega, \Sigma(\omega))$  of

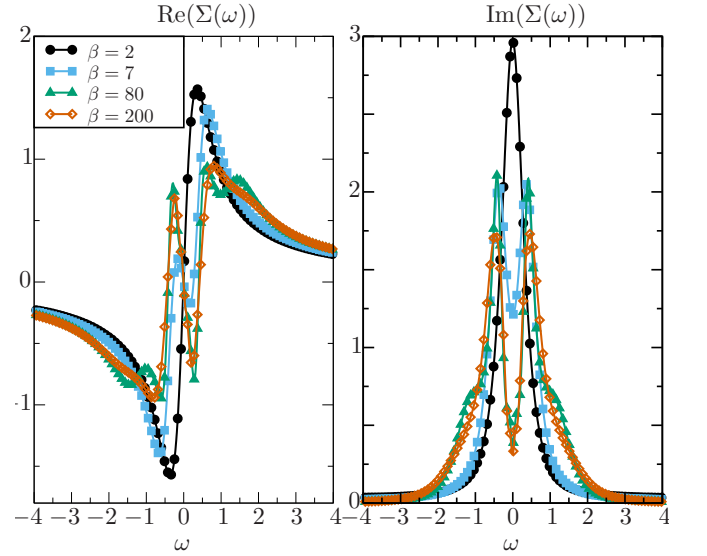


FIG. 8. (Color online) Real and imaginary part of the self-energy  $\Sigma(\omega)$  in different temperature regimes for  $U = 2$ .  $\text{Im}(\Sigma(\omega))$  shows a simple lorentzian shape for  $\beta = 2$  in the local moment regime. Crossing over to the Kondo regime we see the development of a two peak structure. Since  $\Sigma(z)$  is a holomorphic function its real and imaginary part are linked via the Kramers-Kronig relations.

Eq. (3). Fig. 8 shows the self-energy – which is non-vanishing only on the impurity site – in different temperature regimes. Since  $\Sigma(z)$  is a holomorphic function its real and imaginary part are linked via the Kramers-Kronig relations, therefore we find the peak-structure-like features of the imaginary part as zero-crossings in the real part. The apparent symmetry of the self-energies is due to the kernel we have used for the analytical continuation procedure, starting from the imaginary part of the Green's function in Matsubara frequencies as input data. Since we have for the quantity  $\Sigma'$  that

$$\Sigma'(i\omega_n) = \int_{-\infty}^{\infty} d\omega \frac{\text{Im}(\Sigma'(\omega))}{i\omega_n - \omega} \quad (7)$$

its imaginary part is

$$\text{Im}(\Sigma'(i\omega_n)) = -\omega_n \int_{-\infty}^{\infty} d\omega \frac{\text{Im}(\Sigma'(\omega))}{i\omega_n^2 + \omega^2}, \quad (8)$$

which is symmetric in  $\omega$ . Note that  $\Sigma$  and  $\Sigma'$  are linked via a simple rescaling. The temperature dependence of the self-energy documents the crossover from a single peak to a three-peak structure in the impurity spectral function shown in Fig. 7. At temperature scales above the Hubbard  $U$ , correlations effects are not important and the self-energy essentially vanishes such that the impurity spectral function reduces to the non-interacting one with a single central peak pinned at the Fermi energy due to particle-hole symmetry. Lowering the temperature, we observe the formation of three zero crossings

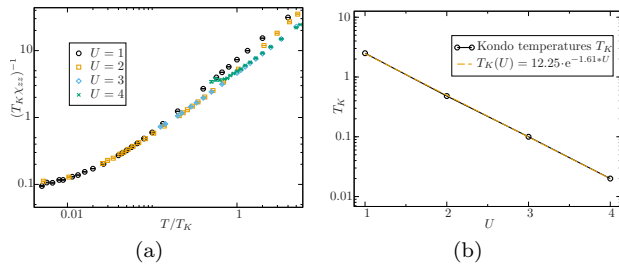


FIG. 9. (Color online) The data for estimating the Kondo temperature  $T_K$  for the parameters  $V = 0.5$  and  $\lambda = 0.1$ . Since  $\chi_{zz}$  is a universal function with  $T_K$  as the only parameter we show in (a) a data collapse of the data for different values of  $U$ . The data points roughly lie on the same function, with the  $U = 1$  points extending to the lowest relative temperatures. (b) shows in a log-plot the obtained Kondo temperatures with its dependence on  $U$ . It shows an exponential dependence on the interaction  $U$  that is expected for the symmetric Anderson model.

in  $\text{Re}(\Sigma)$ . Two are roughly located at  $\omega = \pm U/2$ , are heavily damped since  $\text{Im}(\Sigma)$  is large for those frequencies, and correspond to the upper and lower Hubbard features. The central zero crossing corresponds to the Kondo resonance. It has a narrow line shape and hence has a small value of  $\text{Im}(\Sigma)$ . That these central crossings have the same slope is somehow expected, since the slope should be proportional to the Kondo temperature of the system<sup>27</sup>.

### A. Estimating the Kondo temperature

To get an estimate of the involved Kondo temperatures  $T_K$  we carried out a data collapse in Fig. 9a of the susceptibilities shown in Fig. 6b. from Fig. 9a. It is known that the susceptibility of the Kondo model should be a universal function

$$T_K \chi_{zz} = F\left(\frac{T}{T_K}\right) \quad (9)$$

with  $T_K$  as the only scaling parameter<sup>28</sup>. We find the numerical values for the inverse Kondo temperature  $\beta_K = T_K^{-1}$

$U$	1	2	3	4
$\beta_K$	0.4	2.08	10	50

With the Kondo temperatures at hand we performed a cross check of the obtained values of  $T_K$  and assumed the validity of the asymptotic behaviour of the Kondo temperature for the symmetric Anderson model, given by

$$T_K \propto e^{-\frac{U}{8V^2\rho_0}}, \quad (10)$$

with the density of states  $\rho_0$ <sup>28</sup>. Note that for the Kane-Mele model in the considered parameter range, the Fermi

velocity of the edge state is set by the spin-orbit coupling. Hence  $\rho_0 \propto 1/\lambda$ . The straight line in the log-plot of Fig. 9b indeed confirms this behaviour. Additionally, another cross-check is available by means of the impurity spectral functions of Fig. 7. For  $U = 2$  we have an inverse Kondo temperature of  $\beta_K \approx 2.1$  which is consistent since somewhere in the range  $\beta = 2$  and  $\beta = 10$  the Kondo resonance starts to build-up at  $\omega = 0$ . For  $U = 4$  we get  $\beta_K = 50$  which is again consistent with the data for the spectral function.

### B. High-temperature regime

The high-temperature regime is defined by the lack of any visible structure in the dot's spectral function.  $\beta = 0.1$  in Fig. 7a is a good example, it shows just some lorentzian peak around  $\omega = 0$ . With the presence of the small parameter  $\beta U$  it is obvious that any interaction-induced correlation effects to the spectral functions are negligible. Therefore in this regime the spectral function is that of the uncorrelated system. Since all correlation effects are thermally washed out, the notion of a self-energy is meaningless and hence the self-energy contribution  $C_n(r, \omega, \Sigma(\omega))$  in Eq. (3) vanishes. Therefore, the lattice spectral functions look indistinguishable to the non-interacting case Fig. 5a. Since we are considering the particle-hole symmetric point, the occupancy of the impurity site is pinned to half-filling. Hence in the absence of interactions the double occupancy  $\langle n_{\uparrow}^d n_{\downarrow}^d \rangle$  takes the value 0.25. As apparent in Fig. 6a this value is approached as  $\beta \rightarrow 0$ . Finally, in this high-temperature limit the spin susceptibility shows a  $1/T$  behaviour as apparent from Fig. 6b.

### C. Local Moment regime

The formation of a local moment is at best characterized by the quantity

$$\frac{\langle n_{\uparrow}^d n_{\downarrow}^d \rangle}{\langle n_{\uparrow}^d \rangle \langle n_{\downarrow}^d \rangle}. \quad (11)$$

Since as mentioned previously the denominator of the above equation is pinned to 0.25 by particle-hole symmetry, the formation of the local moment boils down to the suppression of the double occupancy. We will associate a characteristic energy scale of this regime by the dip in the double occupancy of Fig. 6a. The local moment regime corresponds to the regime where the Hubbard bands at  $\omega \approx \pm \frac{U}{2}$  develop in the dot's spectral function. In Fig. 7a,  $\beta = 2$  is a good example of that. At these intermediate temperatures we have one occupied spin state below the Fermi energy at  $-\frac{U}{2}$  with a single electron. This gives rise to essentially a free spin- $\frac{1}{2}$  degree of freedom: a local moment. The energy scale at which the double occupancy is enhanced before saturating marks the onset

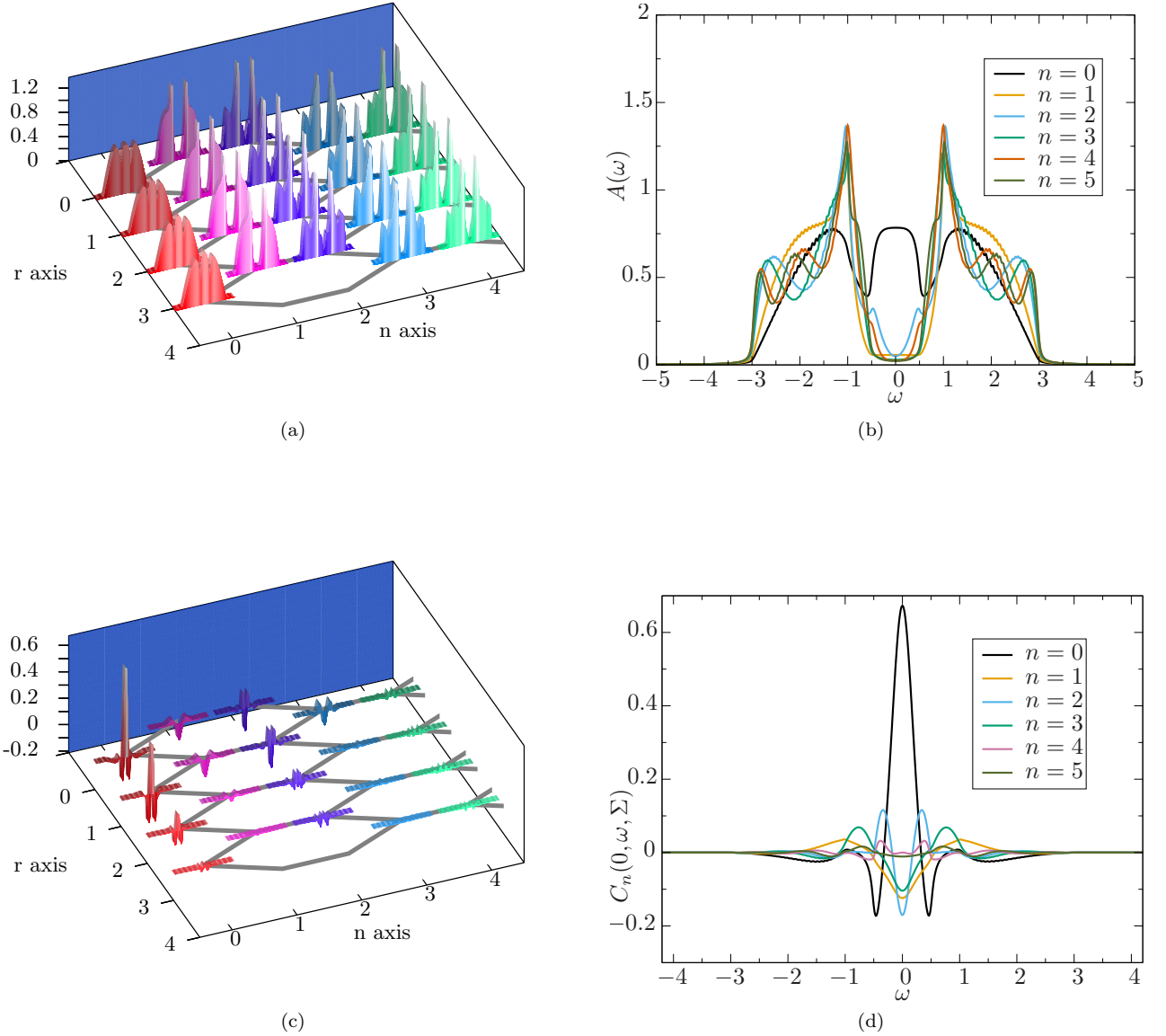


FIG. 10. (Color online) The spectra for the local moment regime at  $\beta = 2, U = 2, V = 0.5$  and  $\lambda = 0.1$ . (a) shows all spectral functions around the impurity, whereas (b) shows a cut of the spectral functions along  $r = 0$ . (c) and (d) show the self-energy contribution  $C_n(r, \omega, \Sigma(\omega))$ .  $C_n(r = 0, \omega, \Sigma(\omega))$  is shown in (d). A neat thing is that the contribution  $C$  due to the self-energy seems to exactly cancel the effects of  $B$ , the hybridization of the impurity with the bath, since the contribution in e.g. Fig. 10d has opposite sign of Fig. 5d.

of the super exchange scale. This scale is set by  $V^2/U$  for our particle-hole symmetric impurity problem. In the context of the helical liquid the spin-flip scattering generated by the super-exchange scale corresponds to single particle back scattering. These processes will hence reduce the conductance as noted in ref.<sup>10</sup>. In the local moment domain, the site resolved single particle spectral function of the edge and bulk states in Fig. 10a show no

sign of Kondo screening. In particular there is no deflection of the edge current perceivable. Fig. 12b shows that the change of  $A_n(r, \omega)$  relative to some very distant point of reference has a very small amplitude. Due to Eq. (3) this means an approximate cancellation of the hybridisation effect from Fig. 5d with the now present self-energy effect shown in Fig. 10d. The edge state is in that sense restored to the true boundary of the lattice as

if no impurity were present. This confirms the robustness of the edge state to a free local moment at least in view of the spectral functions. Nevertheless we expect the conductance through this edge state to decrease in this regime due to the possible backscattering spin-flip processes which is now available due to the impurity<sup>29</sup>. Lowering the temperature further should break this match and deform the edge state again, with the emergence of the Kondo resonance at  $\omega = 0$  in the impurity's spectral function.

#### D. Kondo regime

Lowering the temperature further we enter the Kondo regime. The prominent signature of this regime is the emergence of the Kondo resonance in the dot's spectral functions as seen for example in Fig. 7a at  $\beta = 200$ . The Kondo resonance shows up as a dip in the local spectral function of the edge state electrons at the position of the impurity ( $r = 0$  and  $n = 0$ ) as seen in Fig. 11b. The origin of these spectral features lies in the formation of the Kondo singlet which entangles the impurity spin with the spins of the surrounding electrons. On an energy scale set by the Kondo temperature we expect the impurity site to act as a potential scatterer and hence lead to the deflection of the edge current into the bulk. As apparent, the dip in the spectral weight at  $n = 0$  in Fig. 11d(b) is accompanied by the emergence of a *peak* at  $n = 1$  and  $n = 2$ . At this very low temperature scale,  $T/T_K \simeq 0.01$ , it is this deflection of the edge state discussed by Maciejko et al.<sup>10</sup> which restores the conductance to unitarity in the limit  $T \rightarrow 0$ . Although we have decreased the temperature by two magnitudes the form of the change in Fig. 11d still looks the same, only its magnitude has decreased. But of course now the self-energy term  $C$  and the hybridization term  $B$  do not match anymore as nicely as for  $\beta = 2$ . Hence there is not a full cancellation of the hybridization effect. A further decrease of the temperature should bring us deeper into the Kondo regime with a deflection of the edge state around the impurity as predicted by Maciejko et al.<sup>10</sup>. This confirms that, to the outside world, the singlet state of a magnetic impurity and bath electrons has the same low-energy features as plain potential scattering. We only expect this circumvention of the edge state on an energy scale set by the Kondo temperature  $T_K$ , since beyond this energy scale the equivalence to a potential scatterer is not tenable<sup>30</sup>. Note that since the width of the Kondo resonance is of the order of  $T_K$ , the dip in the bulk spectral functions is of the same size. On the other hand, the width of the edge state is given by the spin-orbit coupling  $\lambda > T_K$ . Fig. 12 shows the change attributable to the impurity measured against a very distant point in the same *orbital*  $n$ :  $\Delta_n(r, \omega) = A_n(r, \omega) - A_n^0(\omega)$ . We see the strong local effect of a potential scatterer in Fig. 12a. In Fig. 12b we see that a correlated impurity at  $\beta = 2$  has a negligible effect on the bath. This corresponds to the local moment

regime. As the temperature drops below the Kondo scale (see the data sets at  $\beta = 7$  in Fig. 12c and at  $\beta = 200$  in Fig. 12d) the same deflection of the edge current as observed for the potential scatterer emerges.

### VI. SPATIALLY RESOLVED DOT BULK SPIN SPIN CORRELATION FUNCTIONS

To provide a different point of view on our study of the Kondo cloud in the bath system that does not rely on an analytic continuation procedure we now turn our attention towards the site resolved spin spin correlation functions

$$\langle S_d^z S_c^z(r, n) \rangle \quad (12)$$

between the impurity spin  $S_d^z = \frac{1}{2} (n_\uparrow^d - n_\downarrow^d)$  and a spin located at a particular site  $S_c^z(r, n) = \frac{1}{2} (n_{r,n,\uparrow} - n_{r,n,\downarrow})$  of a conduction electron. This enables us to define the Kondo cloud as the region of substantial entanglement of the impurity spin with a particular bath site. This is complementary to our previous results where we have defined the Kondo cloud as the region where the edge state is suppressed.

#### A. A 2D overview

First, we consider the non-interacting case and find non-negligible correlations that are confined to the edge of the system. Along the edge the spin spin correlations decay as  $r^{-2}$  as already pointed out in Ref.<sup>31,32</sup> for a 1D system of electrons. Clearly, this power law holds only in the zero temperature limit and at finite temperature an exponential decay sets in beyond the thermal length scale  $\xi_T \propto v_F \beta$  ( $v_F$  is the Fermi velocity). This similarity to the one-dimensional case provides yet another confirmation of the 1D nature of the edge state.

The local moment regime just shows a small amount of correlation in Fig. 15 since due to the high temperature all long-range effects are destroyed. This is in contrast to the behaviour of the spectral functions in Fig. 10a where we see no signature of the impurity in the bath system. If we now lower the temperature into the Kondo regime in Fig. 13 we see that the effect of the impurity mostly extends into the helical liquid in the lower edge and develops some spatial structure.

#### B. Correlation functions along the edge

We now focus our attention on the correlations along the edge as a function of temperature, Hubbard interaction and spin-orbit coupling  $\lambda$ . Borda et al.<sup>31</sup> have studied the spatial behaviour of the spin spin correlation

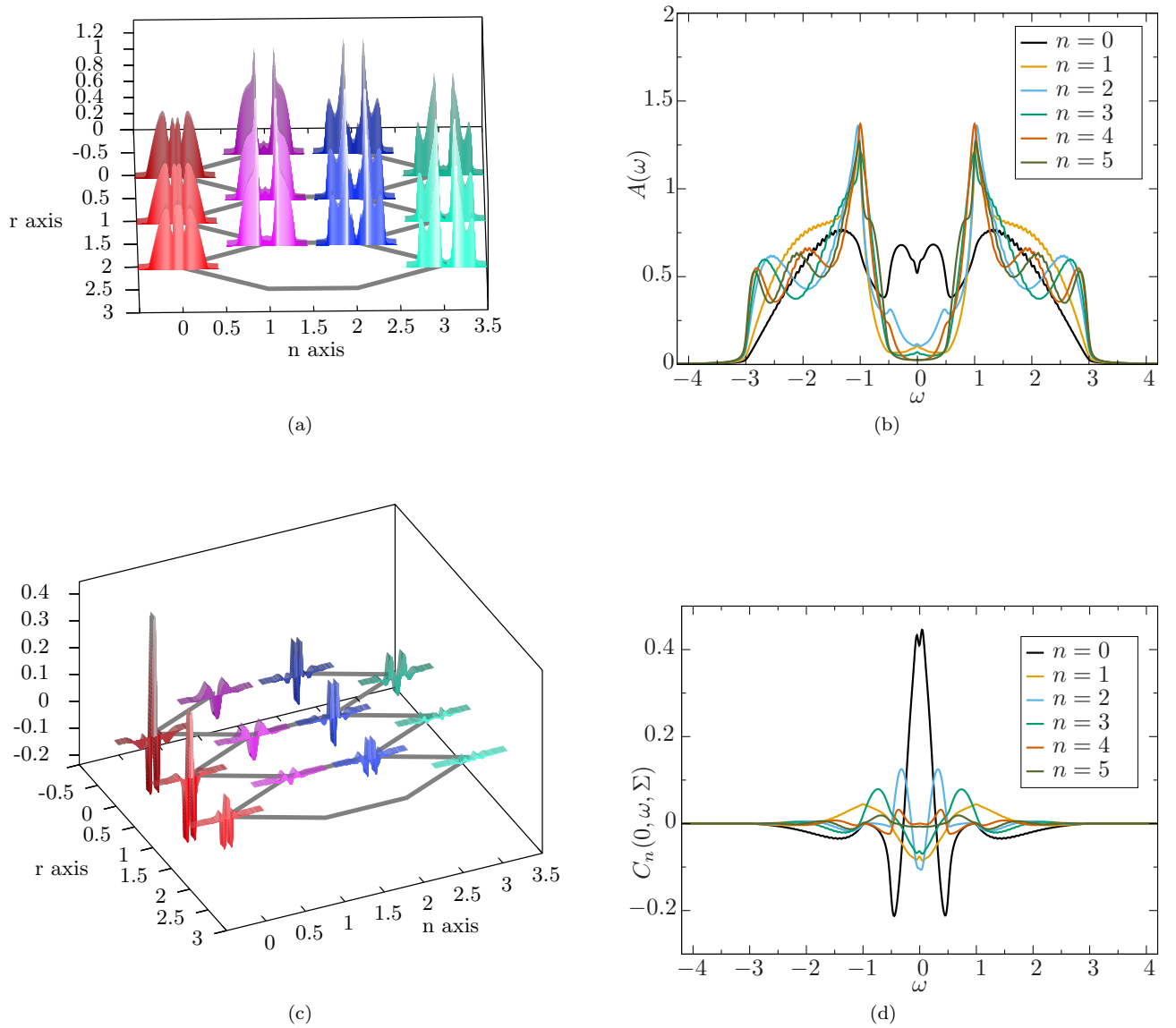


FIG. 11. (Color online) For the parameters  $\beta = 200, U = 2, V = 0.5$  and  $\lambda = 0.1$ , (a) shows a frontal view on the full spectral functions. The dip at the impurity is visible as well as the progression to the full edge state at the edge. (b) shows a cut of the same spectral functions now for increasing  $n$ . The displacement of the edge into the bulk is visible. (c) and (d) show the effect due to the self-energy  $C_n(r, \omega, \Sigma(\omega))$ . Especially figure (d) shows that in comparison with Fig. 10d the functional form of  $C$  seems to be the same although we have increased  $\beta$  by two magnitudes, but the amplitude is reduced from about 0.6 to 0.4.

functions of an Anderson impurity embedded in a one-dimensional wire as bath system. They observed at a distance of  $\xi_K \approx v_F \beta_K$  a crossover from an  $r^{-1}$  behaviour to an  $r^{-2}$  behaviour. For finite temperatures they predict the onset of an exponential decay at  $\xi_T \approx v_F \beta$ . Their study shows that the spatial decay is oscillating with a wave vector  $k \propto k_F = \pi$ . It can already be guessed from the 2D overviews that our system does not show oscil-

lations, which is consistent since  $\cos(2k_F) = 1$ . Fig. 14 shows that the general trend of these predictions made for a 1D chain of electrons also holds for the 1D helical liquid of the edge state of a topological insulator if we perform an analysis similar to Ref.<sup>11</sup>. In Fig. 14, (a) we find the dependence on the Fermi velocity, which is expected to be proportional to the spin-orbit coupling  $\lambda$ . In the plot for  $\lambda = 0.2$  the exponential falloff is shifted outside



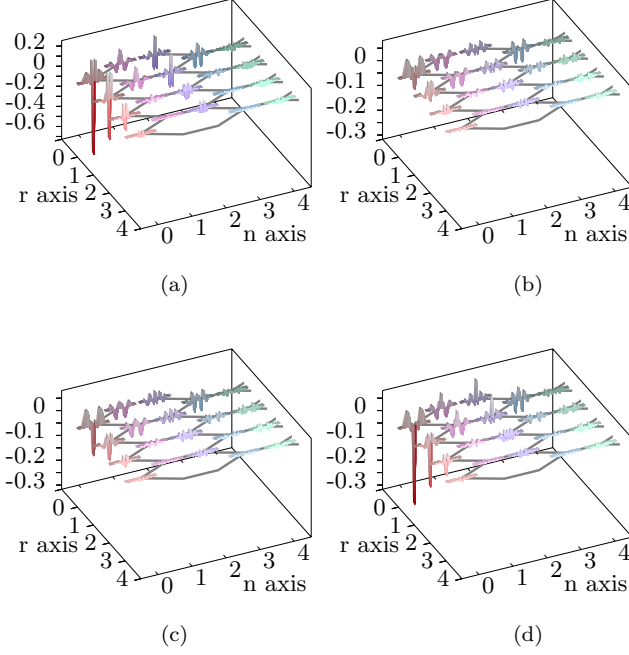


FIG. 12. Here we show the changes to the spectral functions in the vicinity of the impurity relative to some very distant reference point that feels no effect of the impurity. This corresponds to the quantity  $\Delta_n(r, \omega) = A_n(r, \omega) - A_n^0(\omega)$ . (a) shows the changes due to an uncorrelated impurity. (b) is the change in the local moment regime at  $\beta = 2$ . Note the small amplitude of  $\Delta$ , which means that in this regime the bath feels only a negligible effect of the impurity. (c) is in the Kondo regime for  $\beta = 7$ . (d) is in the Kondo regime for  $\beta = 200$ . Note that only (b) - (d) share the same scale on the  $\Delta_n(r, \omega)$  axis.

of the visible part of the edge channel, although the plot for  $\lambda = 0.1$  and  $\lambda = 0.2$  are at the same temperature. In this plot we already have introduced a couple of lines that are meant as guides to the eye. The yellow dashed lines denote the exponential decay that sets in beyond the thermal length scale  $\xi_T \propto v_F \beta$ . The straight dashed magenta lines denote the power law decay  $r^{-2}$  that is present at distances  $\xi_K > r > \xi_T$ . Finally, the straight dashed orange lines denote the  $r^{-1}$  decay that is present for  $r < \xi_K$ <sup>33</sup>. We see that for  $\lambda = 0.2$  the crossover from a  $r^{-1}$  behaviour to a  $r^{-2}$  decay is approximately shifted from  $r \approx 7$  to  $r \approx 16$  and the thermally induced exponential suppression of the spin spin correlation happens much later. We can estimate the thermal cutoff scale by fitting exponentials (the yellow dashed lines),  $e^{-\frac{r}{\xi_T}}$ , to the tails of the plots for  $\beta = 100$  and we find a consistent value of  $\xi_T \approx 8.7$  for all values of  $U$ . A more detailed analysis of the temperature dependence for the point  $U = 2$  is found in Fig. 15. In Fig. 14 (b) and (c) we can compare the temperature effects for  $U = 3$  and we see that at twice the temperature the exponential decay is not visible anymore. Comparing the plots from

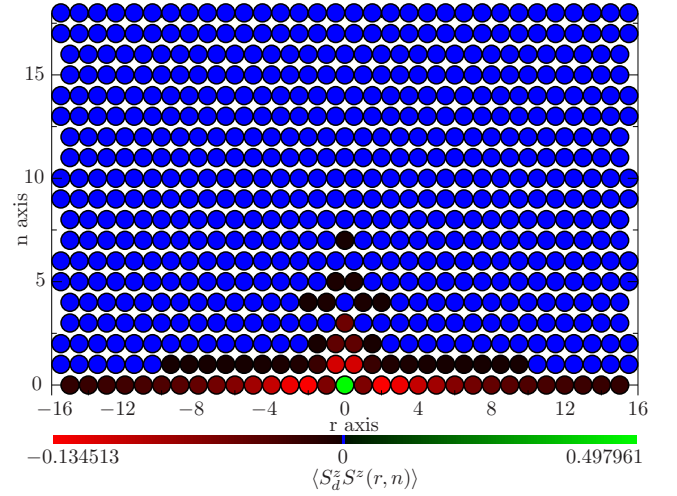


FIG. 13. (Color online) A 2D overview of the color-coded correlation function  $\langle S_d^z S_c^z(r, n) \rangle$  with the full spatial dependence at  $\beta = 100, \lambda = 0.1$  and  $U = 2$ . The impurity is the green spot at  $(r, n) = (0, 0)$  in the middle of the lower edge. Positive values are shades of green, negative values are shades of red and neutral values are blue. The color coding is linear. Note that this does not mean a linear perception of the color values. The comparatively long chain of sites having various shades of red at the bottom of the diagram is the extent that the correlation reaches into the edge state. The correlation extends comparatively far into the edge state but is almost immediately suppressed away from the edge state.

(a) to (d) we can trace the shift of the cross-over from an  $r^{-1}$  behaviour to an  $r^{-2}$  decay with increasing  $U$  and therefore with the Kondo temperature. Fig. 14 (c) also shows the independence of the cross-over point of the algebraic decay due to the Kondo effect with respect to the external temperature.

## VII. SUMMARY

We have studied a magnetic impurity coupled to a helical edge state as modeled by a Kane-Mele Hamiltonian on a slab geometry. Due to time reversal symmetry the effective action of the impurity orbital (see Eq. (5)) has precisely the same form as the generic SIAM such that the local physics is identical. In particular the Hubbard scale marks the appearance of a local moment which couples magnetically via the superexchange scale  $J \propto V^2/U$  to the conduction electrons. Below the Kondo temperature  $T_K$ , the magnetic moment is screened due to the formation of an entangled singlet state of the magnetic impurity and conduction electrons. We have shown these commonalities numerically with the double occupancy, the spin susceptibility and determined the Kondo temperature with a data collapse.

The differences to generic Kondo physics are non-local. As shown in Ref.<sup>12</sup>, if the interactions along the helical edge are not too strong, spin-flip single-particle backward

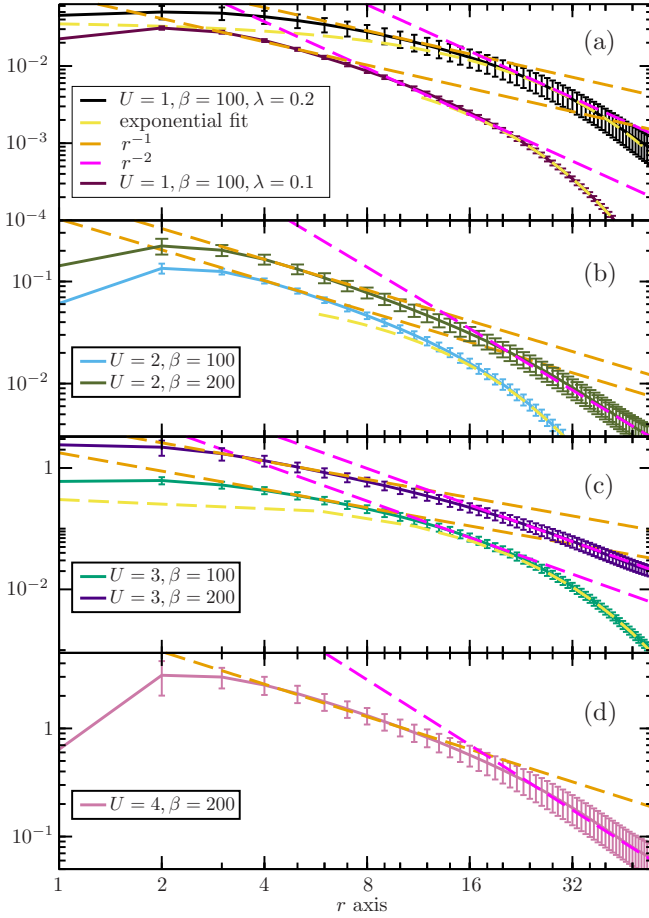


FIG. 14. (Color online) The spatial dependence of the correlation between the impurity's spin and the spin of a site of the edge  $|\langle S_d^z S_c^z(r, n) \rangle|$  with a hybridization of  $V = 0.5$ . Diagram (a) shows the dependence on the Fermi velocity at  $U = 1$  of the cross-over point from an  $r^{-1}$  to an  $r^{-2}$  behaviour,  $\xi_K$ , as well as of the point  $\xi_T$  where the decay crosses over into an exponential law. Note that for  $\xi_K = v_F \beta_K$  both the Fermi velocity and Kondo temperature depend on  $\lambda$ :  $v_F \propto \lambda$  and  $\beta_K \propto \exp(\frac{1}{\lambda})$ . In the graph for  $\lambda = 0.2$  the exponential falloff is shifted outside of the visible lattice although the temperature is kept constant. The dashed lines are guides to the eye and are explained in the main text. Diagrams (b) - (d) are at  $\lambda = 0.1$ . In diagram (b) we show data for higher  $T_K$  at  $U = 2$ . We see that for the higher temperature  $\beta = 200$  the thermal decay at the end of the plot is shifted outside of the visible part of the lattice and we can clearly identify the regimes with power law like behaviour. In the diagram for  $\beta = 100$  the  $r^{-1}$  decay is already dominated by the thermal decay. Figure (c) and (d) show that further increments of  $U$ , which gives higher values of  $\beta_K$ , shifts the cross-over point to larger distances.

scattering processes are expected to be irrelevant, such that in the low temperature limit the conductance should reach the unitarity limit. The mechanism which allows this to occur is the deflection of the edge state into the bulk, thus avoiding the Kondo singlet. By computing the temperature dependence of the site resolved density

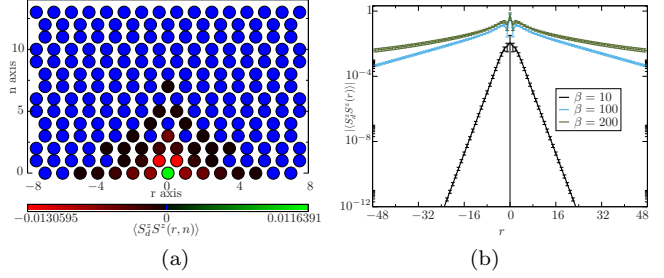


FIG. 15. (Color online) (a) shows the spin spin correlation functions in the local moment regime. Due to the rather high temperature we see that the correlation effects are quickly suppressed. Additionally, the absolute value of the correlations is an order of magnitude lower. The right figure, (b), provides a more detailed view of  $|\langle S_d^z S_c^z(r, 0) \rangle|$  at  $U = 2$ , but at different values of  $\beta$  in a logarithmic plot. Here we can notice the mirror symmetry around the impurity. We see that for  $\beta = 10$ , which is in the local moment regime (compare the spectral functions Fig. 7a), the decay of the correlation function is immediately exponential. This is consistent with the quick suppression in the left figure. Decreasing the temperature to  $\beta = 100$  we see that the exponential decay sets in at around  $\xi_T \approx 8$  whereas for  $\beta = 200$  at  $\xi_T \approx 16$ .

of states by an analytic continuation of the impurity self-energy to real frequencies, we were able to follow the temperature dependence of the edge mode and in particular its deflection into the bulk due to the emergence of the Kondo singlet. Complementary information on the extent of the Kondo singlet – without resorting to an analytical continuation – was also obtained by computing the spatial dependence of the spin spin correlation functions between the local moment and conduction electrons. At low temperatures the spin spin correlations do not extend significantly into the bulk and exhibit a power law decay along the edge. In particular, as a function of temperature, we can observe the thermal cutoff scale  $\xi_T \propto v_F \beta$  beyond which exponential decay sets in, as well as the characteristic cross-over scale around  $\xi_K \propto v_F / T_K$  from an  $r^{-1}$  to an  $r^{-2}$  law. This cross-over scale provides a measure of the Kondo screening cloud. Of significant interest is an explicit calculation of the temperature dependence of the conductance along the edge. In particular, in the local moment regime, where we observe no deflection of the edge state, one expects a decrease of the conductance due to back-scattering spin-flip processes off the impurity spin. Below the Kondo scale, the deflection of the edge state along the new boundary of the system – as defined by the topology of the Kondo cloud – should restore the conductance to its unitarity limit.

## VIII. ACKNOWLEDGMENTS

We especially thank M. Bercx and M. Weber for proof-reading the article. We thank T. C. Lang for the figure of the honeycomb lattice. We acknowledge support from

DFG Grant No. AS120/4-3. We thank the LRZ Munich and the Jülich Supercomputing Centre for generous allocation of CPU time. DJL thanks the university of New Mexico — where part of this work has been carried out — for hospitality. We thank Martin Hohenadler, Thore Posske and Masud Haque for fruitful discussions.

### Appendix A: Analytical continuation

The analytic continuation of the Matsubara Green's function  $G(n, k, i\omega_n)$  to the real frequency axis is a notoriously hard problem and requires potentially large amounts of computer time. For Monte Carlo data, experience shows that the most reliable spectra can be obtained using the stochastic maximum entropy method<sup>34,35</sup> for analytic continuation. This method, however, makes use of a Monte Carlo simulation to find the best spectrum and has to be performed for every pair of indices  $(n, k)$  individually. Clearly, this increases the computational effort substantially. In order to circumvent this problem, we propose to adopt an idea that has been successfully used in the context of the dynamical cluster approximation (DCA)<sup>36</sup>: Instead of the Green's function, we calculate the analytic continuation of the self-energy. The reason why this is beneficial is that the self-energy matrix has only one non-vanishing and diagonal  $2 \times 2$  spin block  $\Sigma(z)$  corresponding to the impurity site and leads to the special form of Dyson's equation:

$$\begin{pmatrix} G_{\vec{r},\vec{r}}(z) & G_{\vec{r},d}(z) \\ G_{d,\vec{r}}(z) & G_{d,d}(z) \end{pmatrix} = \begin{pmatrix} G_{\vec{r},\vec{r}}^0(z) & G_{\vec{r},d}^0(z) \\ G_{d,\vec{r}}^0(z) & G_{d,d}^0(z) \end{pmatrix} + \begin{pmatrix} G_{\vec{r},\vec{r}}^0(z) & G_{\vec{r},d}^0(z) \\ G_{d,\vec{r}}^0(z) & G_{d,d}^0(z) \end{pmatrix} \begin{pmatrix} 0 & 0 \\ 0 & \Sigma(z) \end{pmatrix} \begin{pmatrix} G_{\vec{r},\vec{r}}(z) & G_{\vec{r},d}(z) \\ G_{d,\vec{r}}(z) & G_{d,d}(z) \end{pmatrix}. \quad (\text{A1})$$

Obviously, the knowledge of  $\Sigma(z)$  on the real axis is therefore sufficient to obtain the full interacting Green's function matrix  $G(\omega + i\eta)$  for the whole lattice as the noninteracting Green's function  $G^0$  can be calculated exactly with little difficulty by virtue of the resolvent formalism.

Solving equation (A1) for  $\Sigma(z)$  yields

$$\Sigma(z) = G_{d,d}^0(z)^{-1} - G_{d,d}(z)^{-1}. \quad (\text{A2})$$

As  $G_{d,d}(i\omega_n)$  can be calculated in CT-INT, we can therefore obtain  $\Sigma(i\omega_n)$ . In order to analytically continue  $\Sigma(z)$  to the real axis, we have to study its asymptotic behaviour for large frequencies. Starting from the asymptotic series for  $G_{d,d}^{(0)}(i\omega_n)$

$$G_{d,d}^{(0)}(i\omega_n) = \sum_{k=1}^{\infty} \frac{a_k^{(0)}}{(i\omega_n)^k}, \quad (\text{A3})$$

we obtain through inversion:

$$\begin{aligned} \Sigma(i\omega_n) &= (a_2 - a_2^0) + \frac{1}{i\omega_n} \frac{a_2^2 - (a_2^0)^2 + a_1 a_3 - a_1 a_3^0}{a_1} \\ &\quad + \mathcal{O}\left(\frac{1}{(i\omega_n)^2}\right). \end{aligned} \quad (\text{A4})$$

This result can be obtained by truncating equation (A3) at different orders and one indeed finds out that higher terms of the Green's function's asymptotic series<sup>37</sup> do not contribute to the first two terms of the self-energy.

In order to employ the stochastic maximum entropy method for  $\Sigma(z)$  directly, we introduce a slightly different quantity as already shown in reference 36:

$$\Sigma'(z) = \frac{[\Sigma(z) - (a_2 - a_2^0)] a_1}{a_2^2 - (a_2^0)^2 + a_1 a_3 - a_1 a_3^0}. \quad (\text{A5})$$

This quantity has exactly the same properties as the Green's function itself, namely that its asymptotic series starts with  $\frac{1}{i\omega_n}$ , the corresponding spectral function has a sum rule  $\int d\omega A_{\Sigma}(\omega) = \pi$  and that it does not have a constant term.

In principle, these properties could be corrected for in the maximum entropy procedure but the quantities  $a_2$  and  $a_3$  can only be obtained up to a statistical error-bar and therefore the correct inclusion of these errors is very cumbersome. Performing the transformation (A5) is therefore a very straightforward procedure, as the thoroughly bootstrapped covariance matrix of  $\Sigma'$  will contain all uncertainties stemming from the CT-INT calculation.

The calculation of the constants in the asymptotic series of the self-energy is a straightforward calculation of moments<sup>38</sup> of the spectral function  $A(\omega)$  corresponding to the Green's function  $G_{d,d}$  and yields for  $A_{\Sigma'}^{\sigma}(\omega)$

$$a_2 - a_2^0 = U \langle d_{-\sigma}^{\dagger} d_{-\sigma} \rangle - \frac{U}{2}. \quad (\text{A6})$$

$$\begin{aligned} \frac{(a_2^0)^2 - a_2^2 + a_1(a_3 - a_3^0)}{a_1} = \\ UV \left( \langle a_{0,-\sigma}^{\dagger} d_{-\sigma} \rangle - \langle d_{-\sigma}^{\dagger} a_{0,-\sigma} \rangle \right) \\ + U^2 \langle d_{-\sigma}^{\dagger} d_{-\sigma} \rangle - U^2 \langle d_{-\sigma}^{\dagger} d_{-\sigma} \rangle^2. \end{aligned} \quad (\text{A7})$$

At half filling,  $\langle d_{\sigma}^{\dagger} d_{\sigma} \rangle = \frac{1}{2}$ , so the constant term  $a_2 - a_2^0$  of the self-energy vanishes.

### Appendix B: Diagonal $G_{d,d}$ due to TRI

Since  $[H, T] = 0$ , the operators  $H$  and  $T$  have a common basis in which they are diagonal. In the case that  $T^2 = -1$  holds (which is the case if the total spin is of the half-integer type) we have for every state  $e_1^{\sigma} = |a\rangle$  an

orthogonal state  $e_2 = T|a\rangle$ . In these basis states  $T$  has the matrix representation

$$T = \begin{pmatrix} 0 & \mathbb{1} \\ -\mathbb{1} & 0 \end{pmatrix} \quad (\text{B1})$$

where  $\mathbb{1}$  denotes the identity matrix acting in the respective sub-sector of the state. By that notation we have essentially just renamed the states of the Hilbert space.  $T$  is diagonalized by

$$U = \frac{1}{\sqrt{2}} \begin{pmatrix} \mathbb{1} & i\mathbb{1} \\ i\mathbb{1} & \mathbb{1} \end{pmatrix} \quad (\text{B2})$$

with two eigenvectors named  $|+\rangle$  and  $|-\rangle$ .  $U$  also block-diagonalizes  $H$  and hence the Green's function matrix is block-diagonal in the  $|+\rangle$  and  $|-\rangle$  basis since propagation with  $H$  will not generate matrix elements between the orthogonal sub-spaces.

$$G = \begin{pmatrix} G^{++} & 0 \\ 0 & G^{--} \end{pmatrix}. \quad (\text{B3})$$

Transforming  $G$  back to the original basis we have

$$G = UGU^\dagger = \frac{1}{2} \begin{pmatrix} G^{++} + G^{--} & iG^{++} - iG^{--} \\ -iG^{++} + iG^{--} & G^{++} + G^{--} \end{pmatrix}. \quad (\text{B4})$$

To show that the off-diagonals of this matrix vanish in the sub-space of this matrix where the impurity lives, we consider the impurity Green's function  $G_{d,d}$  in the  $|+\rangle$  and  $|-\rangle$  basis. Then, using time-reversal symmetry,

$$THT^{-1} = H \quad (\text{B5})$$

we have for  $\tau > 0$ ,

$$\begin{aligned} G_{d,d}^{s,s}(\tau) &= \text{Tr} (e^{-\beta H} d_s^\dagger(\tau) d_s) \\ &= \text{Tr} (e^{-\beta THT^{-1}} d_s^\dagger(\tau) d_s) \\ &= \text{Tr} (Te^{-\beta H} T^{-1} e^{-\tau H} d_s^\dagger e^{\tau H} d_s) \\ &= \text{Tr} (e^{-\beta H} e^{-\tau H} T^{-1} d_s^\dagger T e^{\tau H} T^{-1} d_s T) \end{aligned} \quad (\text{B6})$$

using  $T^{-1} d_s T = s d_{-s}$  (the impurity lacks a momentum quantum number) we have

$$\begin{aligned} G_{d,d}^{s,s} &= s^2 \text{Tr} (e^{-\beta H} d_{-s}^\dagger(\tau) d_{-s}) \\ &= G_{d,d}^{-s,-s}. \end{aligned} \quad (\text{B7})$$

Therefore we have  $G_{d,d}^{+,+} = G_{d,d}^{-,-}$  thereby ensuring that the off-diagonals in Eq. (B4) vanish. This in turn gives the diagonality of an impurity Green's function  $G_{d,d}$  just due to time reversal symmetry.

<sup>1</sup> C. L. Kane and E. J. Mele, "Quantum Spin Hall Effect in Graphene," *Phys. Rev. Lett.* **95** (Nov, 2005) 226801. 1

<sup>2</sup> M. Hohenadler, Z. Y. Meng, T. C. Lang, S. Wessel, A. Muramatsu, and F. F. Assaad, "Quantum phase transitions in the Kane-Mele-Hubbard model," *Phys. Rev. B* **85** no. 11, (Mar., 2012) 115132, [arXiv:1111.3949 \[cond-mat.str-el\]](#). 1

<sup>3</sup> M. Hohenadler and F. F. Assaad, "Luttinger liquid physics and spin-flip scattering on helical edges," *Phys. Rev. B* **85** no. 8, (Feb., 2012) 081106, [arXiv:1110.3322 \[cond-mat.str-el\]](#).

<sup>4</sup> Z. Y. Meng, T. C. Lang, S. Wessel, F. F. Assaad, and A. Muramatsu, "Quantum spin liquid emerging in two-dimensional correlated Dirac fermions," *Nature (London)* **464** (Apr., 2010) 847–851, [arXiv:1003.5809 \[cond-mat.str-el\]](#).

<sup>5</sup> M. Hohenadler, T. C. Lang, and F. F. Assaad, "Correlation Effects in Quantum Spin-Hall Insulators: A Quantum Monte Carlo Study," *Phys. Rev. Lett.* **106** no. 10, (Mar., 2011) 100403, [arXiv:1011.5063 \[cond-mat.str-el\]](#).

<sup>6</sup> W. Wu, S. Rachel, W.-M. Liu, and K. Le Hur, "Quantum spin Hall insulators with interactions and lattice anisotropy," *Phys. Rev. B* **85** (May, 2012) 205102. 1

<sup>7</sup> M. Hohenadler and F. F. Assaad, "Correlation effects in two-dimensional topological insulators," *Journal of Physics Condensed Matter* **25** no. 14, (Apr., 2013) 143201, [arXiv:1211.1774 \[cond-mat.str-el\]](#). 1

<sup>8</sup> C. Xu and J. E. Moore, "Stability of the quantum spin Hall effect: Effects of interactions, disorder, and  $\mathbb{Z}_2$  topology," *Phys. Rev. B* **73** (Jan, 2006) 045322. 1

<sup>9</sup> C. Wu, B. A. Bernevig, and S.-C. Zhang, "Helical Liquid and the Edge of Quantum Spin Hall Systems," *Phys. Rev. Lett.* **96** (Mar, 2006) 106401. 1

<sup>10</sup> J. Maciejko, C. Liu, Y. Oreg, X.-L. Qi, C. Wu, and S.-C. Zhang, "Kondo Effect in the Helical Edge Liquid of the Quantum Spin Hall State," *Phys. Rev. Lett.* **102** no. 25, (June, 2009) 256803, [arXiv:0901.1685 \[cond-mat.mes-hall\]](#). 1, 3, 7, 8

<sup>11</sup> T. Posske, C.-X. Liu, J. C. Budich, and B. Trauzettel, "Exact results for the Kondo screening cloud of two helical liquids," *Phys. Rev. Lett.* **110** (Jan, 2013) 016602, [arXiv:1207.7081 \[cond-mat.mes-hall\]](#). 9

- <sup>12</sup> J. Maciejko, “Kondo lattice on the edge of a two-dimensional topological insulator,” *Phys. Rev. B* **85** no. 24, (June, 2012) 245108, [arXiv:1204.0017](#) [[cond-mat.str-el](#)]. 10
- <sup>13</sup> K. T. Law, C. Y. Seng, P. A. Lee, and T. K. Ng, “Quantum dot in a two-dimensional topological insulator: The two-channel Kondo fixed point,” *Phys. Rev. B* **81** (Jan, 2010) 041305. 1
- <sup>14</sup> X.-Y. Feng, W.-Q. Chen, J.-H. Gao, Q.-H. Wang, and F.-C. Zhang, “Anderson impurity in a helical metal,” *Phys. Rev. B* **81** no. 23, (June, 2010) 235411, [arXiv:0910.3031](#) [[cond-mat.str-el](#)]. 1
- <sup>15</sup> Q.-H. Wang, D. Wang, and F.-C. Zhang, “Electronic structure near an impurity and terrace on the surface of a three-dimensional topological insulator,” *Phys. Rev. B* **81** (Jan, 2010) 035104.
- <sup>16</sup> R. R. Biswas and A. V. Balatsky, “Impurity-induced states on the surface of three-dimensional topological insulators,” *Phys. Rev. B* **81** (Jun, 2010) 233405.
- <sup>17</sup> A. K. Mitchell, D. Schuricht, M. Vojta, and L. Fritz, “Kondo effect on the surface of three-dimensional topological insulators: Signatures in scanning tunneling spectroscopy,” *Phys. Rev. B* **87** (Feb, 2013) 075430, [arXiv:1211.0034](#) [[cond-mat.mes-hall](#)]. 1
- <sup>18</sup> P. W. Anderson, “Localized Magnetic States in Metals,” *Phys. Rev.* **124** (Oct, 1961) 41–53. 1
- <sup>19</sup> A. N. Rubtsov, V. V. Savkin, and A. I. Lichtenstein, “Continuous-time quantum Monte Carlo method for fermions,” *Phys. Rev. B* **72** no. 3, (Jul, 2005) 035122, [arXiv:0411344](#) [[cond-mat](#)]. 1
- <sup>20</sup> E. Gull, A. J. Millis, A. I. Lichtenstein, A. N. Rubtsov, M. Troyer, and P. Werner, “Continuous-time Monte Carlo methods for quantum impurity models,” *Review of Modern Physics* **83** (May, 2011) 349 – 404, [arXiv:1012.4474](#) [[cond-mat.str-el](#)].
- <sup>21</sup> F. F. Assaad and T. C. Lang, “Diagrammatic determinantal quantum Monte Carlo methods: Projective schemes and applications to the Hubbard-Holstein model,” *Phys. Rev. B* **76** no. 3, (2007) 035116, [cond-mat/0702455v2](#). 1
- <sup>22</sup> H. Feldner, Z. Y. Meng, A. Honecker, D. Cabra, S. Wessel, and F. F. Assaad, “Magnetism of finite graphene samples: Mean-field theory compared with exact diagonalization and quantum Monte Carlo simulations,” *Phys. Rev. B* **81** (Mar, 2010) 115416. 2
- <sup>23</sup> D. J. Luitz, F. F. Assaad, and M. J. Schmidt, “Exact diagonalization study of the tunable edge magnetism in graphene,” *Phys. Rev. B* **83** no. 19, (May, 2011) 195432, [arXiv:1103.1645](#) [[cond-mat.str-el](#)].
- <sup>24</sup> M. J. Schmidt, “Bosonic field theory of tunable edge magnetism in graphene,” *Phys. Rev. B* **86** no. 7, (Aug., 2012) 075458, [arXiv:1207.3801](#) [[cond-mat.mes-hall](#)]. 2
- <sup>25</sup> G. A. Fiete, V. Chua, M. Kargarian, R. Lundgren, A. Rüegg, J. Wen, and V. Zyuzin, “Topological insulators and quantum spin liquids,” *Physica E: Low-dimensional Systems and Nanostructures* **44** no. 5, (2012) 845 – 859. 2
- <sup>26</sup> G. Schubert, H. Fehske, L. Fritz, and M. Vojta, “Fate of topological-insulator surface states under strong disorder,” *Phys. Rev. B* **85** (May, 2012) 201105, [arXiv:1203.2628](#) [[cond-mat.str-el](#)]. 3
- <sup>27</sup> F. F. Assaad, “Coherence scale of the two-dimensional Kondo lattice model,” *Phys. Rev. B* **70** no. 2, (July, 2004) 020402, [arXiv:0401096](#) [[cond-mat](#)]. 6
- <sup>28</sup> A. C. Hewson, *The Kondo Problem to Heavy Fermions*. Cambridge University Press, Cambridge, 1997. 6
- <sup>29</sup> F. M. Hu, T. O. Wehling, J. E. Gubernatis, T. Frauenheim, and R. M. Nieminen, “Magnetic Impurity Affected by Spin-Orbit Coupling: Behavior near a Topological Phase Transition,” *ArXiv e-prints* (Jan., 2013) , [arXiv:1301.6501](#) [[cond-mat.str-el](#)]. 8
- <sup>30</sup> P. Nozière, “A fermi-liquid” description of the Kondo problem at low temperatures,” *J. Low Temp. Phys.* **17** (1974) 31. 8
- <sup>31</sup> L. Borda, “Kondo screening cloud in a one-dimensional wire: Numerical renormalization group study,” *Phys. Rev. B* **75** (Jan, 2007) 041307, [arXiv:0611208](#) [[cond-mat](#)]. 8
- <sup>32</sup> H. Ishii, “Spin correlation in dilute magnetic alloys,” *Journal of Low Temperature Physics* **32** (1978) 457–467. 8
- <sup>33</sup> Note that these power-laws are not easily reproduced in a plot of the logarithmic derivative of the same data. Further work to pin down the precise nature of the correlation function is required. 10
- <sup>34</sup> A. W. Sandvik, “Stochastic method for analytic continuation of quantum Monte Carlo data,” *Phys. Rev. B* **57** (May, 1998) 10287–10290. 12
- <sup>35</sup> K. S. D. Beach, “Identifying the maximum entropy method as a special limit of stochastic analytic continuation,” *eprint arXiv:cond-mat/0403055* (Mar., 2004) , [arXiv:cond-mat/0403055](#). 12
- <sup>36</sup> S. Fuchs, E. Gull, M. Troyer, M. Jarrell, and T. Pruschke, “Spectral properties of the three-dimensional Hubbard model,” *Phys. Rev. B* **83** (Jun, 2011) 235113, [arXiv:1012.5950](#) [[cond-mat.str-el](#)]. 12
- <sup>37</sup> Note that the leading constant of the Green’s function is generated by the canonical anticommutation relation of  $d^\dagger$  and  $d$  and is therefore  $a_1 = a_1^0 = 1$ . 12
- <sup>38</sup> For this, remember that the  $\alpha$ th moment of the spectral function can be obtained by the expression
- $$\int_{\mathbb{R}} d\omega \omega^\alpha A_{d,d}(\omega) = (-1)^\alpha < \left[ [d^\dagger, H]_{-, \alpha}, d \right]_+ >, \quad (\text{B8})$$
- with the recursive definition
- $$[A, B]_{-, \alpha} = \left[ [A, B]_{-, \alpha-1}, B \right]_- . \quad (\text{B9})$$
- and
- $$[A, B]_{-, 1} = [A, B]_- \quad (\text{B10})$$